

Corrosion Resistance of Biodegradable Zinc Surfaces Enhanced by UV-Grafted Polydimethylsiloxane Coating

Davide Pupillo, Mark P. Bruns, Lucia H. Prado, Francesco Di Franco, David Böhringer, Anca Mazare, Wolfgang H. Goldmann, Sannakaisa Virtanen,* Monica Santamaria,* and Alexander B. Tesler*

Cite This: <https://doi.org/10.1021/acsbmaterials.4c00503>

Read Online

ACCESS |

Metrics & More

Article Recommendations

Supporting Information

ABSTRACT: Improved living conditions have led to an increase in life expectancy worldwide. However, as people age, the risk of vascular disease tends to increase due to the accumulation and buildup of plaque in arteries. Vascular stents are used to keep blood vessels open. Biodegradable stents are designed to provide a temporary support vessel that gradually degrades and is absorbed by the body, leaving behind healed blood vessels. However, biodegradable metals can suffer from reduced mechanical strength and/or inflammatory response, both of which can affect the rate of corrosion. Therefore, it is essential to achieve a controlled and predictable degradation rate. Here, we demonstrate that the corrosion resistance of biodegradable Zn surfaces is improved by electroless deposition of zinc hydroxystannate followed by UV-grafting with silicone oil (PDMS). Potentiodynamic polarization, electrochemical impedance spectroscopy, respiratory kinetic measurements, and long-term immersion in three simulated body fluids were applied. Although zinc hydroxystannate improves the corrosion resistance of Zn to some extent, it introduces a high surface area with hydroxyl units used to UV-graft PDMS molecules. Our results demonstrate that hydrophobic PDMS causes a 3-fold reduction in corrosion of Zn-based materials in biological environments and reduces cytotoxicity through the uncontrolled release of Zn ions.

KEYWORDS: UV-grafting, polydimethylsiloxane, biodegradable metals, zinc, corrosion resistance



1. INTRODUCTION

The global population is experiencing demographic aging and increased life expectancy owing to advances in health care, improved living conditions, better nutrition, and medical innovations. However, the risk of vascular problems tends to increase with age as it is associated with several changes in the vascular system, including the stiffening of the arteries, decreased elasticity of the blood vessels, and changes in the structure and function of the heart.¹ Atherosclerosis, hypertension, coronary artery disease, heart failure, arrhythmias, peripheral arterial disease, and stroke are all age-related problems that contribute to the development of vascular disease.² In this sense, the accumulation and buildup of plaque in the arteries, consisting of cholesterol, fatty substances, cellular debris, calcium, and fibrin, can cause many of these problems.³

Vascular stents are medical devices used to treat narrowed or blocked arteries. The primary purpose of a stent is to keep a narrowed or blocked artery open and to restore normal blood flow. Such stents are commonly made of metals such as stainless steel, cobalt–chromium alloy (CoCr), nickel–titanium alloy (Nitinol),⁴ or polymeric materials such as polyethylene-*co*-vinyl acetate or poly(lactic-*co*-glycolic acid).⁵ The latter are often used to coat drug-eluting stents, helping to control drug release and minimize the risk of an inflammatory

response.⁶ In recent years, biodegradable metal stents have been developed to be decomposed *in vivo* by body fluids over time, leaving behind healed blood vessels.^{7,8} In general, biodegradable biomedical devices provide support and treatment for a specific period before gradually degrading and being absorbed by the body, eliminating the need for a permanent foreign body.^{9–11}

Among the available alternatives, zinc (Zn) and its alloys have gained attention as biodegradable metals due to their biocompatibility and mechanical strength. Zn is an essential trace element that plays an important role in cell development and growth, the immune system, and the nervous system.¹² In addition, Zn is present in extracellular matrices in bone along with hydroxyapatite,¹³ while numerous enzymes require it as a cofactor for their catalytic function.¹⁴ Although Zn is essential for cellular proliferation, differentiation, and signaling, excessive amounts of Zn ions in the body can have harmful effects on vital organs such as the kidney, liver, spleen, brain,

Received: March 14, 2024

Revised: July 4, 2024

Accepted: July 9, 2024

and heart.¹⁵ Therefore, the biocompatibility and mechanical strength of implants should also correlate with corrosion performance, such as corrosion rate and products.¹⁶ Compared to biodegradable metallic alternatives, Zn-based materials have moderate corrosion rates,¹⁷ and can eliminate many of the severe issues associated with Mg-based materials such as hydrogen generation.¹⁸

Although there have been numerous efforts to study the corrosion mechanism of Zn alloys in biological environments, no consensus has been reached due to the influence of various factors, such as alloying materials, and surrounding conditions such as chemical composition, oxygen concentration, and pH. In addition, *in vitro* results of Zn corrosion have been affected by the choice of test solutions. When exposed to saline solutions such as phosphate buffer saline (PBS) and Hank's solution (HS), Zn exhibited uniform corrosion.¹⁷ Furthermore, the corrosion rate varied between PBS and Ringer's solutions; the latter consists only of inorganic components.¹⁹ When immersed in either blood or plasma, the surface of Zn is passivated by biomolecules and inorganic substances. It is well-known that proteins are the first to interact with implants altering the corrosion performance; however, the overall picture is not clear due to different experimental approaches, and the fact that the effect of proteins varies on different metals and alloys.^{20,21}

A vital alternative for improving the corrosion resistance of metallic substrates is to minimize their direct contact with corrosive media.^{22,23} In this sense, chemical grafting of functional hydrophobic molecules can reduce the initial corrosion rate of metallic surfaces by preventing corrosive ions from reaching the surface. Recently, we have shown that selective UV grafting of polydimethylsiloxane (PDMS, silicone oil) can substantially delay the onset of corrosion of martensitic and carbon steel.²⁴

This study investigates the corrosion performance of coated Zn substrates. The substrates were first deposited by rough zinc hydroxystannate microscale coating, followed by UV-grafting of silicone oil (PDMS). Unlike organotin compounds, tin oxides are generally considered nontoxic.²⁵ While zinc hydroxystannate has been proven to improve corrosion resistance in Cl-containing solutions to some extent,²⁶ large amounts of corroded tin compounds can still cause some health issues.^{27,28} Therefore, the surfaces of zinc hydroxystannate were grafted with hydrophobic PDMS molecules. The corrosion resistance of the Zn substrates was evaluated at each preparation step using potentiodynamic polarization measurements, electrochemical impedance spectroscopy (EIS), respiratory kinetic measurements, and long-term immersion in various simulated body fluids with and without added proteins. Our results demonstrate that the PDMS coating significantly improves the corrosion resistance of Zn samples in simulated body fluids, thereby reducing the cytotoxicity due to uncontrolled Zn release.

2. EXPERIMENTAL SECTION

2.1. Materials. Bare Zn sheets of 0.15 mm thickness (>99.95%) were obtained from Goodfellow, UK. Fetal bovine serum (FBS), penicillin–streptomycin, sodium hydroxide, potassium tin(IV) oxide trihydrate, sodium acetate trihydrate, and sodium pyrophosphate were purchased from Sigma-Aldrich, Germany, and ethanol, acetone, toluene, and silicone oil (500 cSt, polydimethylsiloxane, trimethylsiloxy terminated) were bought from Carl Roth, Germany. Dulbecco's modified eagles' medium (DMEM) with stable glutamine and 1.0 g L⁻¹ glucose was bought from Genaxxon Bioscience and used as

received. Deionized water (DI) with a resistivity of 18.2 MΩ·cm has been used in all experiments.

2.2. ZnSn(OH)₆ Electroless Deposition. Bare Zn substrates were used to deposit on the rough ZnSn(OH)₆ coating. The ZnSn(OH)₆ coatings were grown by chemical conversion coating in a stannate-ion-containing aqueous medium at 82 °C for 30 min. The chemical composition of the bath is presented in Table 1.²⁶ The bath

Table 1. Composition of the Electrolyte Used for the Chemical Conversion Coating Process

bath composition	concentration (g L ⁻¹)
NaOH	10
K ₂ SnO ₃ ·3H ₂ O	50
NaC ₂ H ₃ O ₂ ·3H ₂ O	10
Na ₄ P ₂ O ₇	50

medium was not stirred and was exposed to air during the process. The deposited samples were then removed from the bath, rinsed with DI water, and dried under a stream of N₂.

2.3. UV-PDMS Grafting Procedure. The Zn samples after ZnSn(OH)₆ chemical conversion coating were used as substrates for the grafting of the PDMS coating. These samples were horizontally placed in a glass Petri dish under a quartz cover and concealed by approximately 20 μL cm⁻² silicone oil (PDMS), which was pipetted over the entire sample surface. Subsequently, the samples were illuminated using a medium-pressure ultraviolet (UV) (Hg) lamp at 1 kW (UVAPRINT HPV, Hönle AG, Germany) at a working distance of 30 cm. The emission maxima of this type of lamp are in the UV range, *i.e.*, λ = 320 and 365 nm. A power density at the working distance of ~100 mW cm⁻² was measured at λ = 320 nm using an 1830 C Newport optical power meter equipped with an 818-UV/DB optical power detector and a 1% Newport ND filter. The PDMS-covered substrates were illuminated for 30 min. The remanent, nongrafted oil was dissolved in toluene, and then the samples were washed with ethanol and dried under a stream of N₂.

2.4. Morphology and Physicochemical Characterization. For morphological characterization, a field-emission scanning electron microscope (SEM) (Hitachi FE-SEM S4800) was used, equipped with an energy-dispersive X-ray spectroscope (Genesis, Oxford Instruments). A Jasco FT/IR-4700 spectrometer (Tokyo, Japan), equipped with a Jasco ATR-PRO ONE attachment, a single-bounce ATR with a monolithic diamond, was used. Attenuated total reflectance Fourier-transform infrared (ATR-FTIR) spectra were recorded in the range between 6000 and 220 cm⁻¹ with 64 scans and a resolution of 1 cm⁻¹. Air was measured immediately before the sample and used as a background. In the case of pure silicone oil, a volume of 10 μL was dropped directly on the diamond crystal.

2.5. Contact Angle Measurements. The apparent water contact angle (WCA) measurements were carried out using a contact angle goniometer (Dataphysics OCA25, Germany). A small drop was deposited on the surface, the volume was increased to ~10 μL, and the WCA was measured using KRUSS Advance analysis software and the Laplace–Young model for the sessile droplet.

2.6. Potentiodynamic Polarization. Corrosion experiments were performed in different simulating solutions at 37 °C as HS, DMEM, and DMEM with 10% of FBS (DMEM + FBS) with a three-electrode configuration, where the sample was used as the working electrode, a platinum foil as the counter electrode, and a silver/silver chloride electrode (Ag/AgCl_{sat}) as the reference electrode. For each sample, open-circuit potential (OCP) measurements (Zahner Zennium Electrochemical Workstation) were performed for 30 min; subsequently, a potentiodynamic polarization was carried out from -150 mV *vs* the OCP until 0.5 V *vs* the reference electrode at a scanning rate of 5 mV s⁻¹.

2.7. Electrochemical Impedance Spectroscopy Measurements. EIS measurements were performed in HS, DMEM, and DMEM + FBS solutions at 37 °C with a three-electrode configuration, where the sample was used as the working electrode,

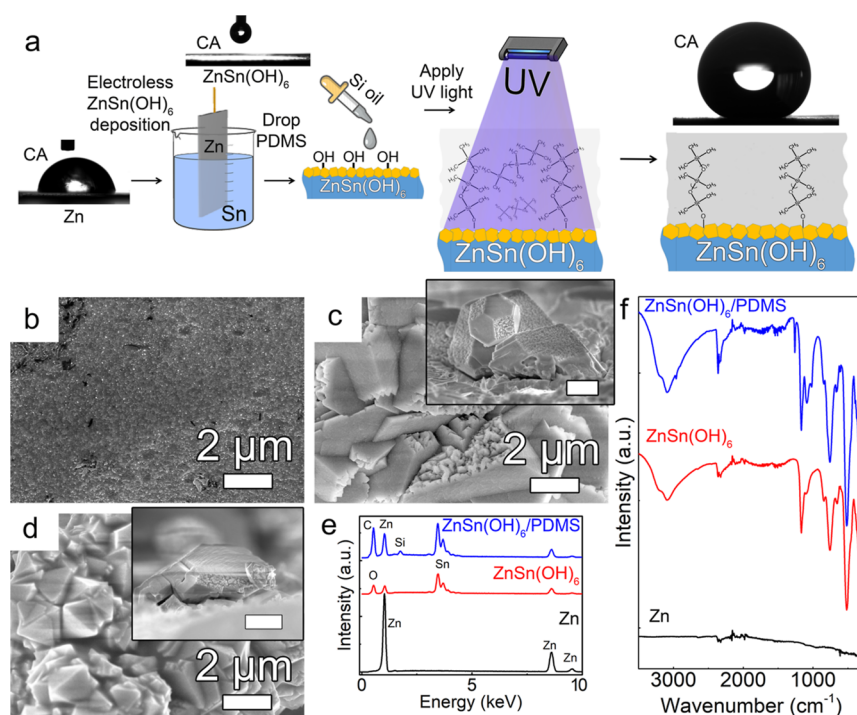


Figure 1. (a) Schematic representation of the PDMS-coated ZnSn(OH)₆ formation process. (b–d) SEM images of bare Zn (b), Zn surface electroless plated by ZnSn(OH)₆ (c), ZnSn(OH)₆-deposited Zn samples coated with PDMS (d). The inset images in (c,d) are cross-sectional SEM images of the corresponding sample with scale bars of 5 μm. (e) Corresponding EDS and (f) FTIR spectra of the samples shown in (b,d).

a platinum foil as a counter electrode, and a silver/silver chloride electrode (Ag/AgCl_{sat}) as a reference electrode. For each solution, open circuit potential (OCP, Zahner Zennium Electrochemical Workstation) was measured for 30 min. EIS measurements were carried out using a Zahner Zennium Electrochemical Workstation at corresponding OCP with a perturbation amplitude of 10 mV in the frequency range between 10 mHz and 100 kHz.

2.8. Respirometry Corrosion Measurements. The total pressure was monitored with a digital pressure sensor (Bosch Sensortec, BMP280, Germany). The H₂ partial pressure was derived, and the O₂ partial pressure was measured with an optical O₂ meter (Piccolo2OEM, Pyroscience, Germany). The solution was stirred at 200 rpm to enable gas exchange between the gas and liquid phases. The presence of H₂ was verified *via* an amperometric H₂ microsensor. A manometric closed setup was used with an electrolyte volume of around 90 mL at room temperature, and the samples have an area of ~8 cm². HS at pH of 7.4 was used as an electrolyte. To perform the respirometric measurements, the hydrogen carbonate was omitted due to the CO₂ formation during its buffering effect, which affected the total pressure measurement. The buffering of the solution was not required, as the monitored pH after 48 h was still 7.4 ± 0.2. Statistical data were calculated from at least three independent experiments for each coating.

2.9. Long-Term Immersion in Simulated Body Fluids. Immersion tests were performed in different simulating solutions at 37 °C as HS, DMEM, and DMEM with 10% of FBS (DMEM + FBS) for 1 week. To reduce bacterial growth, 1% of penicillin–streptomycin was added to the simulating solutions. To estimate the Zn and Sn release in solution, samplings were carried out for each type of solution after 1, 4, and 7 days and diluted 1:10 with 2 wt % nitric acid aqueous solution. A PerkinElmer Optima 2100 DV was used for ICP–OES analysis.

2.10. Biotoxicity Assessment of Coated Zn Surfaces. *Escherichia coli* (*E. coli*, DH-5α) expressing cytoplasmic green fluorescent protein (GFP) were generated using the pGLO bacterial transformation kit (Bio-Rad, Feldkirchen, Germany). The stock culture was generated from an agar stock plate, from which one or two colonies were transferred to a growth medium. All cultures were

incubated overnight at 37 °C in 5 mL of Tryptic Soy Broth growth medium (Becton Dickinson, Heidelberg, Germany) and kept shaking continuously in an orbital shaker at a speed of 150 turns min⁻¹. The concentration of bacteria was measured using UV–vis spectroscopy at a wavelength of 600 nm wavelength (OD_{600 nm}) compared to pure medium (control) and calculated according to the equation: 1.00 OD_{600 nm} = 8 × 10⁸ cfu mL⁻¹.²⁹ Bare and coated Zn samples (15 × 15 mm) were immersed in a diluted GFP-expressing *E. coli* bacteria suspension in 0.5 vol % L-arabinose at an optical density of ~0.30 for 24 h at 37 °C. Material samples for all surfaces were mounted in a 10 cm cell culture dish and immersed in 30 mL LB medium (Carl Roth, Karlsruhe, Germany). After 24 h, the bacteria suspension was removed and samples were washed three times with PBS, followed by imaging at least four positions per sample and 3–4 individual samples per condition. Image stacks (368 × 368 × 22 μm with a voxel size of 0.7 × 0.7 × 2 μm) were acquired at each position using fluorescence microscopy and confocal reflection microscopy. All samples were imaged using an upright laser scanning confocal microscope system (Leica, SP5) with a 20x/1.0NA dip-in objective lens. Image stacks were maximum-projected using Python-based image processing.³⁰ From these images, the bacteria-covered areas were segmented based on the local fluorescence image intensity relative to the overall fluorescence intensity.

3. RESULTS AND DISCUSSION

3.1. Formation of UV-Grafted Zn Surfaces and Their Physicochemical Characterization. Figure 1a presents schematically the formation process of UV-grafted PDMS on Zn surfaces after chemical conversion coating (zinc hydroxystannate, ZnSn(OH)₆). Before electroless deposition of zinc hydroxystannate, Zn substrates were etched in a 5 wt % nitric acid aqueous solution to remove native oxide. The typical top-view SEM image and corresponding energy-dispersive X-ray spectrum of the pre-etched Zn substrates are shown in Figure 1b,e, while the corresponding apparent WCA is presented in Figure 1a. As shown, the WCA of the bare Zn samples is 85.3

$\pm 3.0^\circ$. $\text{ZnSn}(\text{OH})_6$ coating was grown on the pre-etched Zn samples by chemical conversion coating using stannate ions containing aqueous media at 82°C .²⁶ The chemical composition of the bath is summarized in Table 1. During the electroless deposition process, the solution was unstirred and exposed to air. The $\text{ZnSn}(\text{OH})_6$ -deposited Zn samples are termed hereafter as $\text{ZnSn}(\text{OH})_6$. The apparent WCA was measured on the $\text{ZnSn}(\text{OH})_6$ samples demonstrating values below the detection limit of the goniometer, *i.e.*, superhydrophilic surface (Figure 1a). Figure 1c demonstrates the typical top-view SEM image of the morphology of the $\text{ZnSn}(\text{OH})_6$ coated samples. The cross-sectional SEM image indicates a $\text{ZnSn}(\text{OH})_6$ coating thickness of 6–15 μm (Figure S1).

To introduce additional functionalities to the $\text{ZnSn}(\text{OH})_6$ surfaces, polydimethylsiloxane (PDMS, silicone oil) was UV-grafted.²⁴ Plain PDMS is a hydrophobic material that effectively eliminates direct contact of the sample surface with corrosive media.^{31–33} The UV-grafting process is simple, versatile, highly specific, and nondestructive, *i.e.*, the morphology of the deposited zinc hydroxystannate is preserved (Figure S2). Silicone oil was dropped onto the $\text{ZnSn}(\text{OH})_6$ surface, and the samples were exposed to UV light for 30 min. The UV source used in all experiments was a medium-pressure Hg lamp with a peak wavelength of 320 nm. According to the DFT calculations,²⁴ the cleavage of the PDMS molecule is specific and occurs at the trimethylsiloxane terminal groups. Therefore, the UV-grafting step of silicone oil to superhydrophilic $\text{ZnSn}(\text{OH})_6$ surfaces was applied, while the remnant (physisorbed) oil was further dissolved in toluene. Previously, we demonstrated that the UV-grafting of a 500 cSt viscosity PDMS prepared on Si wafer results in the formation of a layer with a thickness of ~ 9 nm (Figure S3).²⁴ The grafting of PDMS was confirmed by SEM, EDS, and contact angle measurements (Figure 1a,d,e). The apparent WCA was measured and found to be $161.4 \pm 5.4^\circ$, *i.e.*, superhydrophobic, for the $\text{ZnSn}(\text{OH})_6/\text{PDMS}$ samples (Figure 1a).

To further characterize UV-grafted PDMS surfaces, ATR-FTIR analysis was employed on bare Zn, $\text{ZnSn}(\text{OH})_6$, and $\text{ZnSn}(\text{OH})_6/\text{PDMS}$ substrates. The FTIR spectra in the wavenumber range of 250–3500 cm^{-1} are shown in Figure 1f. A wide band in the 3100–3300 cm^{-1} region is associated with OH stretching vibrations indicating the presence of hydroxyl groups. The absorption band at 1164 cm^{-1} was due to bending vibrations of the ZnSn–OH bonds. The peaks at 1258, 1083, 1014, and 788 cm^{-1} are the fingerprint for PDMS.³⁴ The PDMS peak at 1258 and a shoulder at 788 cm^{-1} are due to CH_3 deformation and CH_3 rocking in Si– CH_3 , respectively, and the two adjacent peaks at 1083 and 1014 cm^{-1} are due to Si–O–Si asymmetric deformation (Figure S4a). Figure S4b shows the symmetric and asymmetric CH_3 stretching peaks at 2961 and 2902 cm^{-1} , respectively.³⁵ This analysis confirms the successful UV-grafting of the plain silicone oil molecules to the $\text{ZnSn}(\text{OH})_6$ surfaces.

3.2. Electrochemical Corrosion Measurements. It was demonstrated previously that grafted PDMS molecules improve the corrosion resistance of metallic surfaces.^{31,33} To investigate the corrosion performance of the developed coatings, potentiodynamic polarization curve measurements were carried out in HS and DMEM without and with 10% FBS (DMEM + FBS) buffer electrolytes (Figure 2). The presence of zinc hydroxystannate with/without successive surface functionalization induces a reduction in the current density.

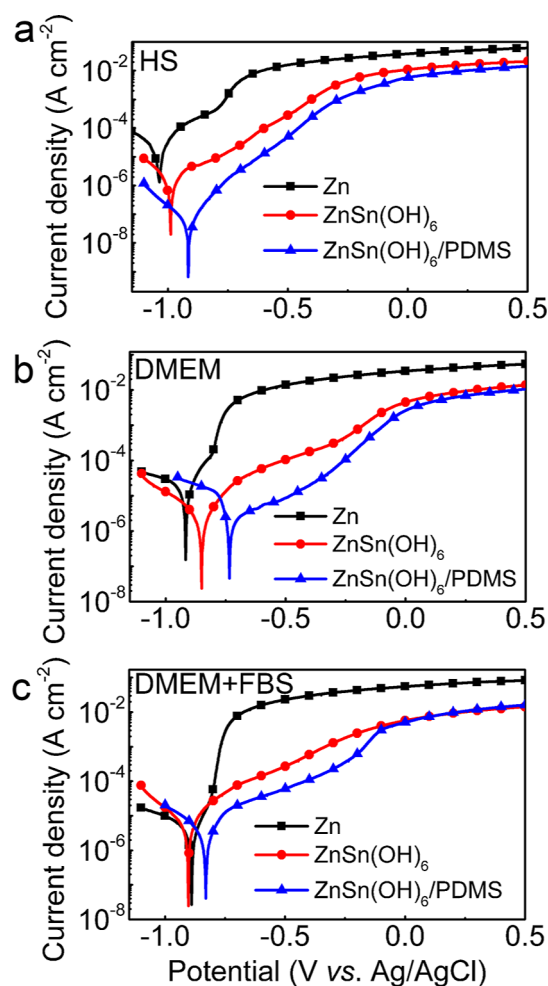


Figure 2. Potentiodynamic polarization curves were measured on bare Zn, $\text{ZnSn}(\text{OH})_6$, and $\text{ZnSn}(\text{OH})_6/\text{PDMS}$ surfaces in (a) HS, (b) DMEM, and (c) DMEM + FBS buffer solutions.

Notably, there is also a substantial shift of the corrosion potential (E_{corr}) to more positive values in all physiological solutions.

The corrosion resistance of the plain and coated Zn surfaces was further evaluated by EIS measurements recorded at the OCP and are shown in the Bode plot in Figure 3. It is evident that the chemical conversion process significantly increases the overall measured electrochemical impedance. The increase is even greater when the $\text{ZnSn}(\text{OH})_6$ samples are UV-grafted with PDMS. The impedance spectra were modeled according to the equivalent circuits reported in Figure S5 and the corresponding fitting parameters are summarized in Tables 2 and 3. For the bare Zn electrodes in all the physiological solutions, the equivalent impedance can be simulated by a parallel connection between a polarization resistance due to the ongoing corrosion process, R_p , and a constant phase element, Q_{dl} , accounting for the nonideal double layer capacitance, in series with the electrolyte resistance, R_{el} (Figure S5a). The estimated R_p is very low for Zn in HS and DMEM, while higher values were measured in DMEM after the addition of FBS. As described in detail in the literature, this can be attributed to the inhibitory effect of proteins.^{21,36} The addition of FBS induces a protective action of the sample surface, thereby enhancing the overall impedance of bare Zn electrodes. The latter can explain the fact that the presence of

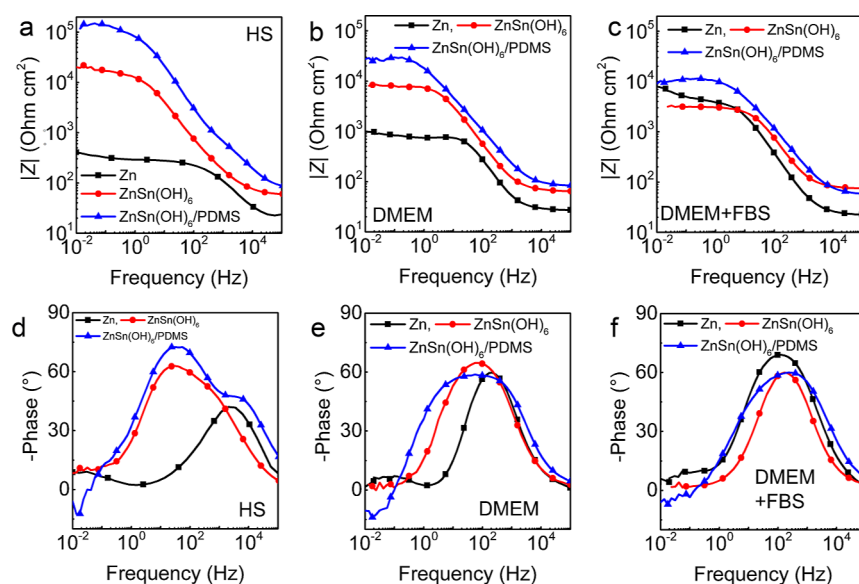


Figure 3. EIS measurements of the bare Zn, ZnSn(OH)₆, and ZnSn(OH)₆/PDMS surfaces in (a,d) HS, (b,e) DMEM, and (c,f) DMEM + FBS buffer solutions.

Table 2. EIS Data is Modeled According to the Equivalent Circuits as Shown in Figure S5a,c

sample/medium	R_{el} [Ω cm ²]	R_p [Ω cm ²]	Q_{dl} [μ S s ⁿ cm ⁻²]	n	L [kHz cm ²]	R_L [Ω cm ²]
Zn in HS	19	275	17	0.71		
Zn in DMEM	28	765	11	0.89		
Zn in DMEM + FBS	23	4468	12	0.84		
ZnSn(OH) ₆ in DMEM	64	8162	8.9	0.82		
ZnSn(OH) ₆ in DMEM + FBS	76	3050	5.6	0.85		
ZnSn(OH) ₆ /PDMS in DMEM	79	3.4×10^4	9.7	0.72	51	3.5×10^5
ZnSn(OH) ₆ /PDMS in DMEM + FBS	70	1.2×10^4	6.3	0.76	45	2.7×10^5

Table 3. EIS Data is Modeled According to the Equivalent Circuit as Shown in Figure S5b,d

sample/medium	R_{el} [Ω cm ²]	Q_{dl} [μ S s ⁿ cm ⁻²]	n	R_1 [Ω cm ²]	R_2 [Ω cm ²]	Q_{cp} [μ S s ⁿ cm ⁻²]	n	L [kHz cm ²]	R_L [Ω cm ²]
ZnSn(OH) ₆ in HS	59	8.6	0.75	1260	1.6×10^4	0.67	0.97		
ZnSn(OH) ₆ /PDMS in HS	85	1.4	0.77	1640	1.4×10^5	0.21	1	6.6×10^3	5.7×10^4

ZnSn(OH)₆ does not change appreciably the impedance values, while the application of a PDMS coating leads to a rise in the impedance.

For the coated samples in DMEM with and without FBS, the spectra can be fitted by the same simple equivalent circuit as for the bare samples (Figure S5a). The higher electrolyte resistance can be explained by the morphology of the coating, which creates a more tortuous pattern for the current line with a consequent increase of R_{el} . The conversion ZnSn(OH)₆ coating increases the polarization resistance, whose values are further increased when PDMS is grafted on top. Notably, when PDMS covers the conversion coatings, a small inductive loop appears at low frequency (*i.e.*, positive phase angle), which can be attributed to adsorption phenomena involving intermediates for H₂ evolution,³⁷ and/or oxidized Zn from the substrate.³⁸

The overall impedance also increases when the Zn samples are tested in HS (Figure 3a). However, a second time constant is required to model the electrical performance of the coated metal in HS (Figure S5b), and the corresponding fit parameters are reported in Table 2. The latter can be explained by the high concentration of phosphate ions present in the HS solution. As soon as Zn is dissolved in the active region that is

still present beneath the conversion ZnSn(OH)₆ coating, Zn phosphate, which is almost insoluble, precipitates leading to a partial sealing of the ZnSn(OH)₆ surface.

Based on these results, we can conclude that upon coating Zn with zinc hydroxystannate, the overall impedance increases in all of the investigated electrolytes, the highest being measured when the chemical conversion is followed by the PDMS coating, while the ZnSn(OH)₆/PDMS samples provided the highest corrosion protection in all three physiological solutions. Here, the ZnSn(OH)₆/PDMS coating reduces the contact time between the aggressive environment (*e.g.*, physiological medium) and the underlying zinc hindering the possibility of the onset of corrosion phenomena.

3.3. Cathodic Kinetics Measured Using the Respirometry Approach. The corrosion kinetics of the bare and coated Zn samples were further investigated by respirometric measurements in modified HS. A detailed description of the method and its application in corrosion measurements can be found in our previous publications,^{39–41} and Section S6 in Supporting Information. Briefly, monitoring the cathodic reactions in aqueous media, specifically the hydrogen evolution reaction (HER) and the oxygen reduction reaction (ORR), allows for the inference of the amount of anodic reaction. The

H_2 partial pressure was derived by monitoring the total pressure, whereas the O_2 partial pressure was measured using an optical O_2 meter. The respective molar changes were calculated using the ideal gas law and then converted to charges using Faraday's law. The dissolved O_2 concentration in the liquid phase was measured using the O_2 meter, while the dissolved H_2 concentration was calculated using Henry's law. The solution was stirred to facilitate gas exchange between the gas and the liquid phases. The presence of H_2 was confirmed by using an amperometric H_2 microsensor. The O_2 partial pressure was monitored in the gas phase. The total O_2 consumption was almost entirely from the gas phase, as is evident from the equilibration of the two phases. Note that for Zn corrosion, in addition to the regular 4-electron ORR pathway, there is also a 2-electron pathway that results in the formation of H_2O_2 .⁴² Since the experimental setup could not detect H_2O_2 , the conversion to anodic charge is imprecise but must be in the range of the two pathways. Therefore, the total cathodic charges were calculated using the 4-electron pathway, which will eventually dominate as H_2O_2 decomposes. In particular, as the concentration increases, the two molecules are likely to react to form O_2 and H_2O , which ultimately contributes to the 4-electron pathway. Assuming that the ORR pathway remains unchanged for the different coatings, the cathodic charges can be used to compare their corrosion rates. However, even in the extreme scenario where peroxide formation is the only process and the coated samples corrode exclusively *via* the 4-electron ORR mechanism, the bare Zn samples would still exhibit significantly higher corrosion rates.

Figure 4a summarizes the respirometric total charge measurements of the Zn, $ZnSn(OH)_6$, and $ZnSn(OH)_6/$

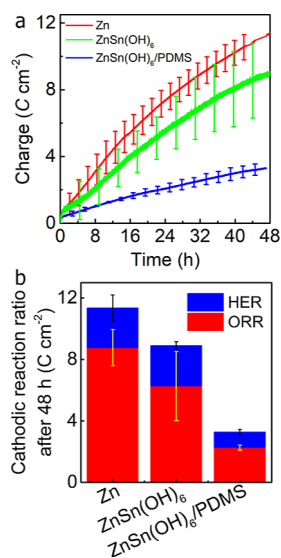


Figure 4. (a) Total cathodic charge densities (ORR + HER) were obtained for 48 h in the modified Hank's electrolyte using the respirometric measurements. (b) Cathodic reaction ratio ORR and HER after 48 h of exposure to the modified Hank's electrolyte.

PDMS samples. The corrosion current density was calculated from the linear fit slope of the total charge density as a function of time and was found to be 52.8, 44.4, and 15.8 $\mu A cm^{-2}$ for bare Zn, $ZnSn(OH)_6$, and $ZnSn(OH)_6/$ PDMS samples, respectively. The latter indicates that the PDMS coating results in a 3-fold reduction of the corrosion rates compared to both the Zn and $ZnSn(OH)_6$ counterparts, which is consistent

with the potentiodynamic polarization and EIS measurements. Figure 4b presents the ratio between HER and ORR for the corresponding samples. While the bare Zn exhibits the highest cathodic charge density, it also shows the highest ORR/HER ratio of $\sim 77\%$. The $ZnSn(OH)_6$ and $ZnSn(OH)_6/$ PDMS samples exhibit the ORR/HER ratio of $\sim 70\%$. It is known that Zn corrodes primarily by ORR in alkaline media, while in neutral electrolytes, it exhibits a mixed ORR and HER response.⁴³ As shown, the difference between Zn and $ZnSn(OH)_6/$ PDMS is substantial. Here, the cathodic reaction difference is attributed to the protective performance of the developed coatings. Although it is known that pH increases due to the ORR during Zn corrosion, we did not observe a significant change in pH of the electrolyte during the experiment. The difference in cathodic reaction ratio could be attributed to a local increase in pH near the sample surface, which could lead to a shift in the ORR ratio in the case of bare Zn.

3.4. Stability of Corrosion Protection. To investigate the long-term corrosion protection of the developed coatings, Zn, $ZnSn(OH)_6$, and $ZnSn(OH)_6/$ PDMS samples were immersed in the physiological buffer solutions for a 1 week. The SEM images after 1 week of immersion show that the surface of bare Zn is damaged due to corrosion, while there is no evidence of corrosion on the surface of the $ZnSn(OH)_6/$ PDMS electrodes despite the long immersion time (Figure 5). The conversion coating is still present with a morphology identical to that of the as-prepared substrates as compared by EDS analysis (Figure 5g–i,l). This result is also supported by the inductively coupled plasma-optical emission spectroscopy (ICP-OES) release test, which allows for the assessment of the Sn^{4+} concentration in physiological solutions following a one-week immersion period. As shown in Figure S9, the Sn ion concentration was negligible. The EDS analysis also reveals that the C and Si peaks are still clearly observed on the $ZnSn(OH)_6/$ PDMS samples (Figure 5). The latter is in accordance with potentiodynamic polarization and EIS measurements confirming the corrosion-protective nature of hydrophobic PDMS molecules. Moreover, the distinct appearance of Ca and P peaks in the EDS spectra of the $ZnSn(OH)_6/$ PDMS samples may indicate the improved formation of calcium phosphates. The latter result is consistent with the literature since it is known that silicones play an important role in bone formation and calcification,⁴⁴ *i.e.*, this is because silicon presents in biological apatite playing a major role in bone biochemistry by initiating the mineralization process. These findings were also confirmed by recording impedance spectra in the physiological buffer solutions at the OCP at 37 °C after 1 week of immersion (Figure S10). The overall impedance does not change appreciably for the coated samples despite the long immersion time.

The release of Zn ions was monitored using ICP on days 1, 4, and 7 of immersion in the investigated physiological solutions. As shown in Figure 6, the presence of $ZnSn(OH)_6$ reduces the release of Zn ions in HS, resulting in the lowest Zn^{2+} concentration. In contrast, the highest concentration of Zn ion was observed in DMEM, where there is still evidence of a beneficial effect of the coating. However, the addition of FBS to the solution results in a Zn ion release rate that appears to be independent of the physiological solution used and unaffected by the coating. These findings can be explained by the different corrosion mechanisms of Zn, which vary depending on the composition of the different simulated body

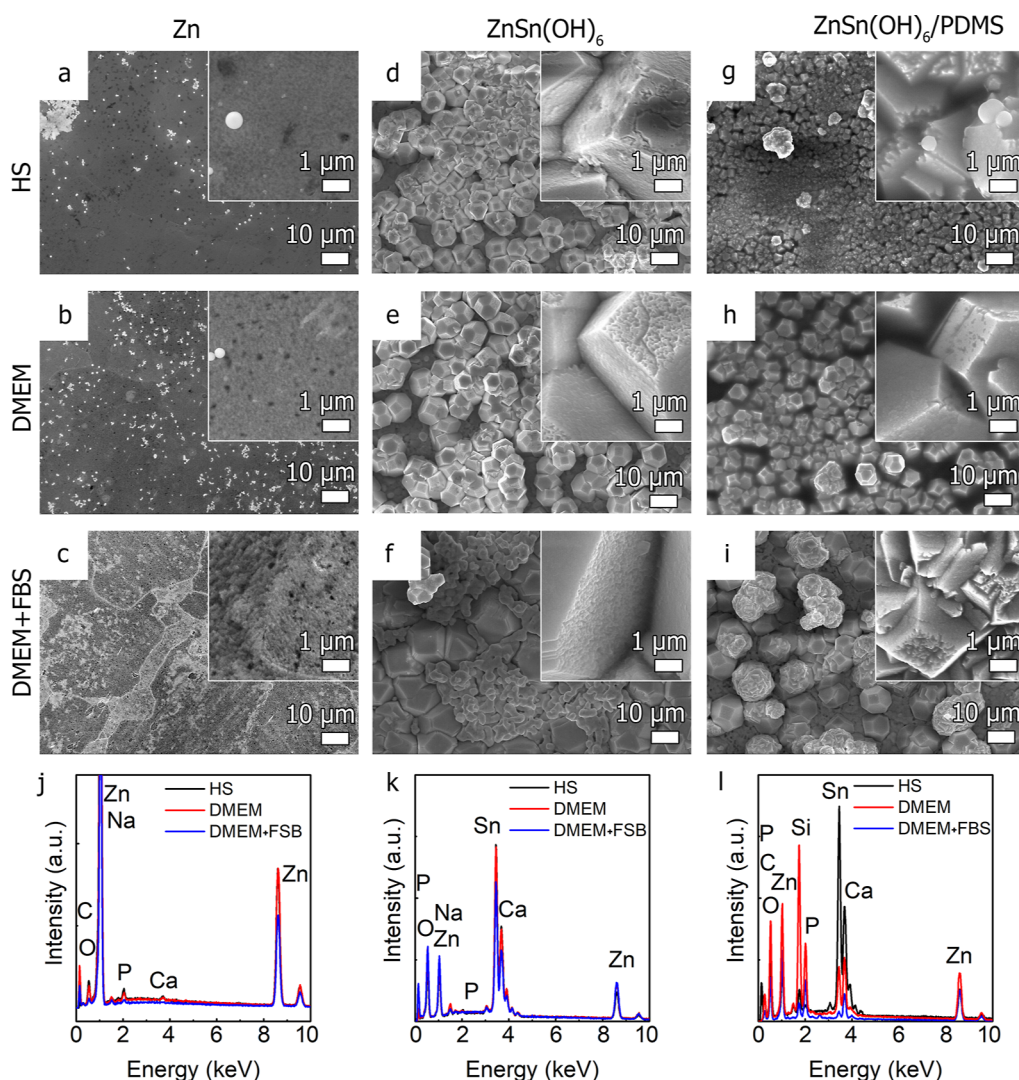


Figure 5. SEM images of Zn, ZnSn(OH)₆, and ZnSn(OH)₆/PDMS samples after 7 days of immersion in (a,d,g,i) HS, (b,e,h,k) DMEM, and (c,f,i,l) DMEM + FBS solutions. (j–l) EDS spectra of Zn (j), ZnSn(OH)₆ (k), and ZnSn(OH)₆/PDMS (l) samples after 7 days of immersion in HS, DMEM, and DMEM + FBS solutions.

fluids used. In HS, the high concentration of phosphate induces the precipitation of Zn phosphate on the metal surface, which has a passivating effect, thus reducing the concentration of free Zn²⁺ in the solution. DMEM contains several amino acids, that can chelate Zn ions, leading to the precipitation of Zn salts. In the presence of FBS (DMEM + FBS), proteins can be adsorbed onto the surface of bare Zn, inhibiting its corrosion.¹⁷

3.5. Toxicity Assessment of Bare and Coated Zn Surfaces Due to Increased Corrosion. The key challenge in the field of biodegradable implant devices is their gradual corrosion to introduce a controllable amount of metal ions into the bloodstream. Although Zn is an essential mineral for several physiological processes including immune function, wound healing, and DNA synthesis, its excessive release due to uncontrolled corrosion can lead to cell toxicity.⁴⁵ To evaluate the toxicity of Zn caused by corrosion in physiological media, it was immersed in a solution of GFP-expressing *E. coli*. Here, *E. coli* is used as a transducer to evaluate the cytotoxicity of Zn ions released into physiological media. This is because Zn has been shown to have an antibacterial effect by inhibiting the uptake of manganese by bacteria, which leads to increased

susceptibility to oxidative stress and reduced bacterial growth. Moreover, an excess of Zn has been demonstrated to be toxic to cells as it selectively deactivates iron–sulfur enzymes in *E. coli*.⁴⁶

The results on the bacterial growth and surface adhesion studies are summarized in Figure 7. As anticipated, both the number of nonmotile bacteria attached to the exposed Zn samples and motile bacteria in the growth medium showed the lowest optical density values due to the increased corrosion rates, indicating that Zn alone has the greatest negative impact on bacterial cells (Figure 7a,d). Both ZnSn(OH)₆ and ZnSn(OH)₆/PDMS coated samples showed higher bacterial adhesion and optical density values of bacterial growth in the medium. This indicates that there was a smaller effect on *E. coli* compared to bare Zn and medium control (Figure 7b–d). However, the bacterial surface coverage varied between the ZnSn(OH)₆ and ZnSn(OH)₆/PDMS surfaces. While a bacterial monolayer is observed on the former (Figure 7b), patchy bacterial assemblies are present on the latter (Figure 7c). This difference in bacterial assembly is attributed to the lower adhesion strength of bacteria to the PDMS-coated surfaces, where UV-grafted silicone oil serves as a lubricating

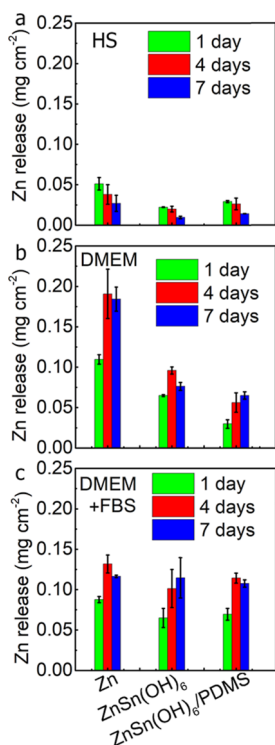


Figure 6. ICP measurements of Zn, ZnSn(OH)₆, and ZnSn(OH)₆/PDMS, surfaces after (a) 1, (b) 4, and (c) 7 days of immersion in (a) HS, (b) DMEM, and (c) DMEM + FBS.

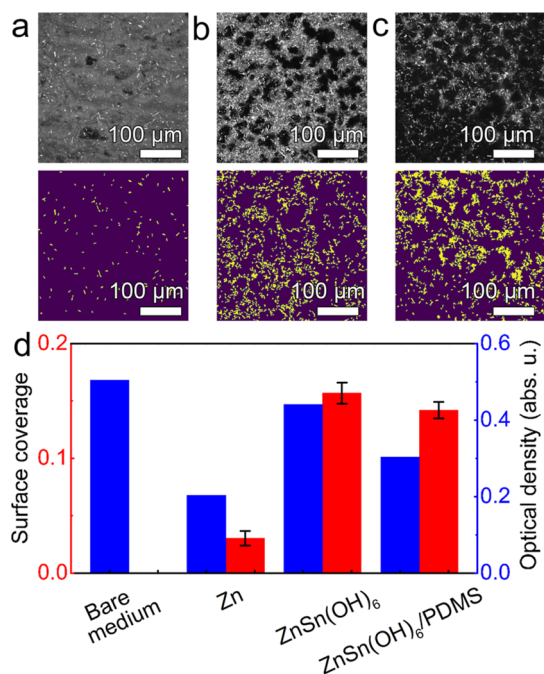


Figure 7. (a–c) Typical raw and processed confocal microscopy images of nonmotile live GFP-expressed *E. coli* on (a) bare Zn, (b) ZnSn(OH)₆, and (c) ZnSn(OH)₆/PDMS samples. (d) Corresponding surface coverage of nonmotile live GFP-expressed *E. coli* on the samples shown in (a–c) and optical density measurements of bacteria growth after 24 h in the growth medium with and without bare and coated Zn samples.

layer. Such patches form during the subtraction and rinse processes, *i.e.*, the exposure of the samples to the liquid–air

interface during their harvesting is enough to partially remove bacteria from the sample surface. The latter is consistent with previous studies.^{24,47}

4. CONCLUSIONS

This study presents a way to enhance the corrosion resistance of biodegradable Zn surfaces in simulated body fluids by the electroless deposition of (i) zinc hydroxystannate followed by (ii) UV-grafting with silicone oil (PDMS). Potentiodynamic polarization, EIS, respiratory kinetic measurements, and long-term immersion were applied in three simulated body fluids with and without added proteins. The results indicate that the electroless-deposited zinc hydroxystannate layer only modestly improves the corrosion resistance of Zn in biological environments; however, it introduces a rough high surface area layer of hydroxyl groups, which are used to graft PDMS molecules by their selective cleavage under UV irradiation. The grafting of hydrophobic PDMS molecules further enhances the corrosion resistance of Zn-based surfaces in biological environments by a reduction in the current density of both the cathodic and the anodic branches and a notable shift of the corrosion potential to more positive values in all physiological solutions. A similar corrosion resistance trend was also observed in EIS measurements, where PDMS-coated samples demonstrated the highest polarization resistance in all three simulated body fluids. The corrosion kinetics was further obtained using a respiratory approach, demonstrating corrosion current densities three times lower for ZnSn(OH)₆/PDMS samples as compared to the bare Zn and ZnSn(OH)₆ counterparts. While immersed in simulated body fluids for 7 days, the PDMS-coated samples demonstrated the enhanced formation of hydroxyapatite since silicones play an important role in bone formation and calcification. Finally, the enhancement of corrosion resistance of the coated Zn samples reduces the cytotoxicity of the released Zn ions, while the adhesion strength of bacteria weakens on PDMS-coated surfaces due to the lubricating effect of the UV-grafted silicone oil.

■ ASSOCIATED CONTENT

Supporting Information

The Supporting Information is available free of charge at <https://pubs.acs.org/doi/10.1021/acsbmaterials.4c00503>.

Figure S1: top-, tilted-view, cross-sectional SEM images and corresponding EDS spectrum of the ZnSn(OH)₆ samples, Figure S2: top-, tilted-, cross-sectional SEM images and corresponding EDS spectrum of the ZnSn(OH)₆/PDMS sample, Figure S3: ellipsometric and XPS depth profile measurements of the UV-grafted PDMS on smooth substrates, Figure S4: ATR-FTIR measurements of plain and ZnSn(OH)₆-deposited Zn samples with and without PDMS coating, Figure S5: EIS data modeled by equivalent circuits, Figure S6: respirometric immersion setup with oxygen measurements in both liquid and gas phases, Figure S7: cathodic charges of ORR and HER for pure Zn, Figure S8: cathodic charges for the ZnSn(OH)₆/PDMS specimens, Figure S9: ICP-OES release test of the Sn⁴⁺ concentration in the physiological solutions, Figure S10: EIS of the bare and coated Zn samples (PDF)

AUTHOR INFORMATION

Corresponding Authors

Sannakaisa Virtanen – Department of Materials Science and Engineering, Institute for Surface Science and Corrosion, Faculty of Engineering, Friedrich-Alexander-Universität Erlangen-Nürnberg, Erlangen 91058, Germany; Email: virtanen@ww.uni-erlangen.de

Monica Santamaria – Dipartimento di Ingegneria, Università di Palermo, Palermo 90128, Italy; orcid.org/0000-0002-8690-4881; Email: monica.santamaria@unipa.it

Alexander B. Tesler – Department of Physics, Biophysics Group, Friedrich-Alexander-Universität Erlangen-Nürnberg, Erlangen 91052, Germany; orcid.org/0000-0003-3425-7667; Email: alexander.tesler@fau.de

Authors

Davide Pupillo – Dipartimento di Scienza Applicata e Tecnologia, Politecnico di Torino, Torino 10129, Italy

Mark P. Bruns – Department of Materials Science and Engineering, Institute for Surface Science and Corrosion, Faculty of Engineering, Friedrich-Alexander-Universität Erlangen-Nürnberg, Erlangen 91058, Germany

Lucia H. Prado – Department of Materials Science and Engineering, Institute for Surface Science and Corrosion, Faculty of Engineering, Friedrich-Alexander-Universität Erlangen-Nürnberg, Erlangen 91058, Germany; orcid.org/0000-0002-6311-5601

Francesco Di Franco – Dipartimento di Ingegneria, Università di Palermo, Palermo 90128, Italy; orcid.org/0000-0002-5722-2881

David Böhringer – Department of Physics, Biophysics Group, Friedrich-Alexander-Universität Erlangen-Nürnberg, Erlangen 91052, Germany

Anca Mazare – Department of Materials Science and Engineering, Institute for Surface Science and Corrosion, Faculty of Engineering, Friedrich-Alexander-Universität Erlangen-Nürnberg, Erlangen 91058, Germany

Wolfgang H. Goldmann – Department of Physics, Biophysics Group, Friedrich-Alexander-Universität Erlangen-Nürnberg, Erlangen 91052, Germany

Complete contact information is available at:

<https://pubs.acs.org/10.1021/acsbiomaterials.4c00503>

Notes

The authors declare no competing financial interest.

ACKNOWLEDGMENTS

A.B.T. thanks the Deutsche Forschungsgemeinschaft (grant number 540989797) for financial support. A.B.T. and W.H.G. thank the Deutsche Forschungsgemeinschaft (grant number 442826449) for financial support. M.P.B. gratefully acknowledges financial support from the Deutsche Forschungsgemeinschaft via the VI 350/13-1. D.B. was funded by the Deutsche Forschungsgemeinschaft (FA 336-12/1, TRR-SFB 225 Projects A01 and C02). M.S. and F.D.F. acknowledge the European Union (NextGeneration EU), for the support through the MUR-PNRR project SAMOTHRACE. Dr. M. Strelb is acknowledged for helpful discussions and support in the development of respirometric techniques. W.H.G. and A.B.T. are indebted to Liz Nicholson (MA) for proofreading the manuscript.

REFERENCES

- (1) North, B. J.; Sinclair, D. A. The Intersection Between Aging and Cardiovascular Disease. *Circ. Res.* **2012**, *110* (8), 1097–1108.
- (2) Lakatta, E. G.; Levy, D. Arterial and Cardiac Aging: Major Shareholders in Cardiovascular Disease Enterprises. *Circulation* **2003**, *107* (1), 139–146.
- (3) Insull, W. The Pathology of Atherosclerosis: Plaque Development and Plaque Responses to Medical Treatment. *Am. J. Med.* **2009**, *122* (1), S3–S14.
- (4) Korei, N.; Solouk, A.; Haghbin Nazarpak, M.; Nouri, A. A review on design characteristics and fabrication methods of metallic cardiovascular stents. *Mater. Today Commun.* **2022**, *31*, 103467.
- (5) Im, S. H.; Im, D. H.; Park, S. J.; Jung, Y.; Kim, D.-H.; Kim, S. H. Current status and future direction of metallic and polymeric materials for advanced vascular stents. *Prog. Mater. Sci.* **2022**, *126*, 100922.
- (6) Marroquin, O. C.; Selzer, F.; Mulukutla, S. R.; Williams, D. O.; Vlachos, H. A.; Wilensky, R. L.; Tanguay, J.-F.; Holper, E. M.; Abbott, J. D.; Lee, J. S.; et al. A Comparison of Bare-Metal and Drug-Eluting Stents for Off-Label Indications. *N. Engl. J. Med.* **2008**, *358* (4), 342–352.
- (7) Li, H.; Zheng, Y.; Qin, L. Progress of biodegradable metals. *Prog. Nat. Sci.: Mater. Int.* **2014**, *24* (5), 414–422.
- (8) Zong, J.; He, Q.; Liu, Y.; Qiu, M.; Wu, J.; Hu, B. Advances in the development of biodegradable coronary stents: A translational perspective. *Mater. Today Bio* **2022**, *16*, 100368.
- (9) Zheng, Y. F.; Gu, X. N.; Witte, F. Biodegradable metals. *Mater. Sci. Eng., R* **2014**, *77*, 1–34.
- (10) Hermawan, H.; Dubé, D.; Mantovani, D. Developments in metallic biodegradable stents. *Acta Biomater.* **2010**, *6* (5), 1693–1697.
- (11) Khan, A. R.; Grewal, N. S.; Zhou, C.; Yuan, K.; Zhang, H.-J.; Jun, Z. Recent advances in biodegradable metals for implant applications: Exploring in vivo and in vitro responses. *Results Eng.* **2023**, *20*, 101526.
- (12) Maywald, M.; Rink, L. Zinc homeostasis and immunosenescence. *J. Trace Elem. Med. Biol.* **2015**, *29*, 24–30.
- (13) Molenda, M.; Kolmas, J. The Role of Zinc in Bone Tissue Health and Regeneration—a Review. *Biol. Trace Elem. Res.* **2023**, *201* (12), 5640–5651.
- (14) McCall, K. A.; Huang, C.-c.; Fierke, C. A. Function and Mechanism of Zinc Metalloenzymes. *J. Nutr.* **2000**, *130* (5), 1437S–1446S.
- (15) Nriagu, J. Zinc Toxicity in Humans. In *Encyclopedia of Environmental Health*, 2nd ed.; Nriagu, J., Ed.; Elsevier, 2019; pp 500–508.
- (16) Hermawan, H. Updates on the research and development of absorbable metals for biomedical applications. *Prog. Biomater.* **2018**, *7* (2), 93–110.
- (17) Liu, L.; Lu, L.; Zhang, H.-J.; Wang, L.-N. Influence of bovine serum albumin on corrosion behaviour of pure Zn in phosphate buffered saline. *J. Mater. Sci.: Mater. Med.* **2021**, *32* (9), 95.
- (18) Tsakiris, V.; Tardei, C.; Clicinschi, F. M. Biodegradable Mg alloys for orthopedic implants – A review. *J. Magnes. Alloys* **2021**, *9* (6), 1884–1905.
- (19) Törne, K.; Larsson, M.; Norlin, A.; Weissenrieder, J. Degradation of zinc in saline solutions, plasma, and whole blood. *J. Biomed. Mater. Res., Part B* **2016**, *104* (6), 1141–1151.
- (20) Virtanen, S. Corrosion of Biomedical Implant Materials. *Corros. Rev.* **2008**, *26* (2–3), 147–171.
- (21) Hedberg, Y. S. Role of proteins in the degradation of relatively inert alloys in the human body. *npj Mater. Degrad.* **2018**, *2* (1), 26.
- (22) Tesler, A. B.; Kolle, S.; Prado, L. H.; Thievensen, I.; Böhringer, D.; Backholm, M.; Karunakaran, B.; Nurmi, H. A.; Latikka, M.; Fischer, L.; et al. Long-term stability of aerophilic metallic surfaces underwater. *Nat. Mater.* **2023**, *22*, 1548–1555.
- (23) Tesler, A. B.; Nurmi, H. A.; Kolle, S.; Prado, L. H.; Karunakaran, B.; Mazare, A.; Erceg, I.; de Brito Soares, I.; Sarau, G.; Christiansen, S.; et al. Predicting plastron thermodynamic stability

for underwater superhydrophobicity. *Commun. Mater.* **2024**, *5* (1), 112.

(24) Tesler, A. B.; Prado, L. H.; Khusniyarov, M. M.; Thievensen, I.; Mazare, A.; Fischer, L.; Virtanen, S.; Goldmann, W. H.; Schmuki, P. A One-Pot Universal Approach to Fabricate Lubricant-Infused Slippery Surfaces on Solid Substrates. *Adv. Funct. Mater.* **2021**, *31* (27), 2101090.

(25) Johnson, W.; Bergfeld, W. F.; Belsito, D. V.; Hill, R. A.; Klaassen, C. D.; Liebler, D. C.; Marks, J. G.; Shank, R. C.; Slaga, T. J.; Snyder, P. W.; Andersen, F. A. Safety Assessment of Tin(IV) Oxide as Used in Cosmetics. *Int. J. Toxicol.* **2014**, *33*, 40S–46S.

(26) Di Franco, F.; Zaffora, A.; Megna, B.; Santamaria, M. Heterogeneous crystallization of zinc hydroxystannate on galvanized steel for enhancing the bond strength at the rebar/concrete interface. *Chem. Eng. J.* **2021**, *405*, 126943.

(27) Louria, D. B.; Joselow, M. M.; Browder, A. A. The Human Toxicity of Certain Trace Elements. *Ann. Int. Med.* **1972**, *76* (2), 307–319.

(28) Yusof, E. N. M.; Ravoof, T. B. S. A.; Page, A. J. Cytotoxicity of Tin(IV)-based compounds: A review. *Polyhedron* **2021**, *198*, 115069.

(29) Myers, J. A.; Curtis, B. S.; Curtis, W. R. Improving accuracy of cell and chromophore concentration measurements using optical density. *BMC Biophys.* **2013**, *6* (1), 4.

(30) Rausch, M.; Böhringer, D.; Steinmann, M.; Schubert, D. W.; Schrüfer, S.; Mark, C.; Fabry, B. Measurement of Skeletal Muscle Fiber Contractility with High-Speed Traction Microscopy. *Biophys. J.* **2020**, *118* (3), 657–666.

(31) Liu, J.; Sun, Y.; Zhou, X.; Li, X.; Kappl, M.; Steffen, W.; Butt, H.-J. One-Step Synthesis of a Durable and Liquid-Repellent Poly(dimethylsiloxane) Coating. *Adv. Mater.* **2021**, *33* (23), 2100237.

(32) Tesler, A. B.; Prado, L. H.; Thievensen, I.; Mazare, A.; Schmuki, P.; Virtanen, S.; Goldmann, W. H. Nontoxic Liquid-Infused Slippery Coating Prepared on Steel Substrates Inhibits Corrosion and Biofouling Adhesion. *ACS Appl. Mater. Interfaces* **2022**, *14* (25), 29386–29397.

(33) Prado, L. H.; Böhringer, D.; Mazare, A.; Sotelo, L.; Sarau, G.; Christiansen, S.; Fabry, B.; Schmuki, P.; Virtanen, S.; Goldmann, W. H.; Tesler, A. B. Silicone-Based Lubricant-Infused Slippery Coating Covalently Bound to Aluminum Substrates for Underwater Applications. *ACS Appl. Mater. Interfaces* **2023**, *15* (26), 31776–31786.

(34) Bao, C.; Xu, K.-Q.; Tang, C.-Y.; Lau, W.-m.; Yin, C.-B.; Zhu, Y.; Mei, J.; Lee, J.; Hui, D.; Nie, H.-Y.; Liu, Y. Cross-Linking the Surface of Cured Polydimethylsiloxane via Hyperthermal Hydrogen Projectile Bombardment. *ACS Appl. Mater. Interfaces* **2015**, *7* (16), 8515–8524.

(35) Pemberger, N.; Huck, C. W.; Bittner, L. K. H. Using Near-Infrared Spectroscopy to Monitor the Curing Reaction of Silicone Adhesives. *Spectroscopy* **2015**, *30*, 8–19.

(36) Talha, M.; Ma, Y.; Kumar, P.; Lin, Y.; Singh, A. Role of protein adsorption in the bio corrosion of metallic implants – A review. *Colloids Surf. B Biointerfaces* **2019**, *176*, 494–506.

(37) Curioni, M.; Salamone, L.; Scenini, F.; Santamaria, M.; Di Natale, M. A mathematical description accounting for the superfluous hydrogen evolution and the inductive behaviour observed during electrochemical measurements on magnesium. *Electrochim. Acta* **2018**, *274*, 343–352.

(38) Kauffman, G. B. Electrochemical Impedance Spectroscopy. By Mark E. Orazem and Bernard Tribollet. *Angew. Chem., Int. Ed.* **2009**, *48* (9), 1532–1533.

(39) Strebl, M.; Bruns, M.; Virtanen, S. Editors' Choice—Respirometric in Situ Methods for Real-Time Monitoring of Corrosion Rates: Part I. Atmospheric Corrosion. *J. Electrochem. Soc.* **2020**, *167* (2), 021510.

(40) Strebl, M. G.; Bruns, M. P.; Virtanen, S. Coupling Respirometric HER and ORR Monitoring with Electrochemical Measurements. *Electrochim. Acta* **2022**, *412*, 140152.

(41) Strebl, M. G.; Bruns, M. P.; Virtanen, S. Respirometric in Situ Methods for Real-Time Monitoring of Corrosion Rates: Part III.

Deconvolution of Electrochemical Polarization Curves. *J. Electrochem. Soc.* **2023**, *170* (6), 061503.

(42) Wroblowa, H. S.; Qaderi, S. B. The mechanism of oxygen reduction on zinc. *J. Electroanal. Chem. Interface Electrochem.* **1990**, *295* (1–2), 153–161.

(43) Thomas, S.; Birbilis, N.; Venkatraman, M. S.; Cole, I. S. Corrosion of Zinc as a Function of pH. *Corrosion* **2012**, *68* (1), 015009-1–015009-9.

(44) Kim, B.-S.; Yang, S.-S.; Yoon, J.-H.; Lee, J. Enhanced bone regeneration by silicon-substituted hydroxyapatite derived from cuttlefish bone. *Clin. Oral Implants Res.* **2017**, *28* (1), 49–56.

(45) Goldmann, W. H. Biosensitive and antibacterial coatings on metallic material for medical applications. *Cell Biol. Int.* **2021**, *45* (8), 1624–1632.

(46) Corbin, B. D.; Seeley, E. H.; Raab, A.; Feldmann, J.; Miller, M. R.; Torres, V. J.; Anderson, K. L.; Dattilo, B. M.; Dunman, P. M.; Gerads, R.; et al. Metal Chelation and Inhibition of Bacterial Growth in Tissue Abscesses. *Science* **2008**, *319* (5865), 962–965.

(47) Abbas, A.; Wells, G. G.; McHale, G.; Sefiane, K.; Orejon, D. Silicone Oil-Grafted Low-Hysteresis Water-Repellent Surfaces. *ACS Appl. Mater. Interfaces* **2023**, *15* (8), 11281–11295.